Fundamental Journal of Modern Physics
ISSN: 2249-9768
Volume 16, Issue 1, 2021, Pages 39-66
This paper is available online at http://www.frdint.com/
Published online December 30, 2021

STRUCTURAL, ELECTRONIC AND OPTICAL PROPERTIES IN STRONGLY CORRELATED COMPOUNDS IN BOTH PrF_3 AND $Sr_{0.75}Pr_{0.25}F_{2.25}$: A DFT + U STUDY

Z. CHOUAHDA[a,*], R. KHEMICI[a,b], H. MERADJI[a] and S. GHEMID[a]

[a]Laboratoire LPR
Département de Physique
Faculté des Sciences
Université Badji
Mokhtar, Annaba
Algérie
e-mail: achouahda@gmail.com

[b]Laboratoire d'Etude et Recherche
des Etats Condensés (LEREC)
Département de Physique
Faculté des Sciences
Université Badji
Mokhtar, Annaba
Algérie

Keywords and phrases: Wien2k, LSDA, LSDA + U, Hubbard, strongly electron-electron correlation, fluorite, praseodymium, optical properties.

*Corresponding author

Received February 18, 2021; Accepted December 13, 2021

Abstract

The structural, electronic and optical properties of both rare earth fluoride PrF_3 and $Sr_{0.75}Pr_{0.25}F_{2.25}$ were studied using density functional theory plus both the local spin density approximation (LSDA) and (LSDA + U) formalism, implemented in the code Wien2k. Electronic properties such as the band structures and the total state densities were calculated. It is found that PrF_3 and $Sr_{0.75}Pr_{0.25}F_{2.25}$ exhibit a conductive energy-gap for the spin up and an insulating for the spin down from both approximations. Optical properties derived from the dielectric function $\varepsilon(\omega)$, such as the refractive index $n(\omega)$, the absorption coefficient $\alpha(\omega)$, the reflectivity $R(\omega)$ and the spectrum $L(\omega)$ which represents the electron energy loss (Electron Energy Loss Spectroscopy, EELS) are studied for the first time for $Sr_{0.75}Pr_{0.25}F_{2.25}$.

1. Introduction

The rare earth or lanthanide family includes the atoms of the periodicals classification ranging from lanthanum $(Z = 57)$ to lutetium $(Z = 71)$ with the electronic structure: $[Xe]4f^N 6s^2$ where N varies from 0 to 14. Rare earth ions occur in divalent or trivalent form. They have more important optical properties than neutral atoms when used as active ions in crystalline matrices for luminescence studies. These ions are mainly in trivalent form: the $6s$ electrons and one $4f^N$ electron of the neutral atom have disappeared. The $4f^N$ electrons are responsible for the optical and magnetic properties of the lanthanide ions. As the electrons of this layer are shielded from the crystalline environment by the outer layers, $4f$ electrons are well localized and there is a strongly electron-electron correlation.

The DFT is not adapted to study all systems and especially rare earth doped materials in its usual form and both LDA and GGA

approximations. To take into account these strong correlations, it is essential to use approximations beyond the LDA or GGA, such as the self interaction correction (SIC) [1] method, hybrid functional [2], DFT + U [3-7], etc. The latter will be used in the present work, to study the strong correlated fluorides doped rare earth [1]. The DFT + U approximation was introduced for the first time by Anisimov [3, 4]. In this approximation, a corrective potential is added to the standard LDA and GGA functions to describe the repulsions between strongly correlated electrons located at the same site (3d in transition metal oxides, 5f in actinide oxides and 4f in the lanthanides). According to the Anderson model [8], the electrons are separated into two subsystems. The first one represents the localized electrons d or f electrons for which Coulomb d-d (f-f) interaction should be taken into account. In the second, the delocalized s, p electrons could be described by using an orbital independent one-electron potential (LDA).

TRF_3 trifluorides such as LaF_3, PrF_3 and CeF_3 isomorphs of the mineral tysonite have excellent electrical performances due to the high mobility of the F^- ion in these materials [9]. As such, they offer numerous application possibilities in electrochemical energy storage and in micro ionic devices: batteries and accumulators, pressure sensors, specific electrodes, etc.

The structure of natural tysonite was initially determined by Oftedal [10] and then by Schlyter [11]. It crystallizes in the hexagonal system with the space group P63/mcm (Z = 6) according to Oftedal [10] and P63/mmc (Z = 2) according to Schlyter [11]. The TRF_3 (TR = La, Ce, Pr, Nd) have been the subject of numerous studies with often contradictory results. The high number of converging results for the trigonal symmetry and the space group $P\bar{3}c1$ suggest that this group is the most likely [11-19]. The miniaturization of laser sources is a subject at the heart of research and is related to the development of

nanotechnologies. Praseodymium appears to be the most suitable rare earth for obtaining RGB (Red-Green-Blue) micro-sources used for image reconstruction by projection. Indeed it presents four interesting transitions for the realization of these micro-sources around 480, 520, 600 and 630 nm [20].

The fluorides strongly substituted in Praseodymium $M_{1-x}\ Pr_x\ F_{2+x}$ ($x \approx 35\%$) (M = Ca, Ba, Sr) [21-23] have been widely studied experimentally in order to determine the spectroscopic properties of the Praseodymium ion in these materials. The present work consists in providing additional or complementary information on Pr^{3+} doped SrF_2 using the Wien2k code [24].

First, the structural properties such as the equilibrium parameter, the compressibility modulus and its derivative are calculated. Then we present the electronic properties such as the band structures and the total and partial state densities using the two approximations LSDA and LSDA + U. Then we evaluate the optical properties derived from the dielectric function $\varepsilon(\omega)$, such as the refractive index $n(\omega)$, the absorption coefficient $\alpha(\omega)$, the reflectivity $R(\omega)$ and the spectrum $L(\omega)$ which represents the electron energy loss (Electron Energy Loss Spectroscopy, EELS).

2. Calculations Details

The calculations have been performed using the full potential augmented linearized plane waves (PF-LAPW) method implemented in the Wien2k code [24] within the framework of the Density Functional Theory (DFT) [25]. LSDA exchange-correlation functions and the combination of LSDA with Hubbard term (LSDA + U) are used. The latter takes into account the exchange and correlation effects of the 4f states of praseodymium. In the augmented linearized plane wave method (FP-LAPW), space is divided into two regions: a region consisting of non-

overlapping spheres surrounding the atomic sites (Muffin-tin spheres) and an interstitial region located between the spheres. Kohn and Sham wave functions are developed in terms of spherical harmonics inside Muffin-tin spheres for a maximum value of $l_{\max} = 10$ and in Fourier series in the interstitial region with a cut-off radius $R_{MT}K_{\max} = 7$ (where R_{MT} is the smallest Muffin-tin radius and $K_{\max}$ is the largest wave vector in the Brillouin zone). The iteration process is repeated until the total energy calculation converges to less than 0.1 mRyd. The number of k-points in the first Brillouin zone has been taken equal to 900 for PrF_3 and 1000 for $Sr_{1-x}Pr_xF_{2+x}$. The solid solutions $M_{1-x}Pr_xF_{2+x}$ ($x \approx 35\%$) (M = Ca, Ba, Sr) are obtained using the Bridgman technique by mixing the fluorides MF_2 (Fluorine) and TRF_3 (Tysonite). Despite the difference between the two structures, there is a high reciprocal solubility of MF_2 (Fluorine) and TRF_3 (Tysonite) and a wide range of fluorine type solid solutions is obtained when the concentration of Praseodymium x is less than 50% [26]. The mixed fluoride $Sr_{1-x}Pr_xF_{2+x}$ was modeled for a selected composition ($x = 0.25$), by repeated super-cells of 13 atoms: the Pr atoms occupy the 8 vertices of the cube (0, 0, 0), the Sr atoms occupy the faces middles (0.5, 0.5, 0), (0.5, 0, 0.5) and (0, 0.5, 0.5) and the F atoms occupy the 8 tetrahedral sites (0.25, 0.25, 0.25); (0.25, 0.75; 0.25); (0.75, 0.25, 0.25); (0.75, 0.75, 0.25); (0.25, 0.25, 0.75); (0.25, 0.75, 0.75); (0.75, 0.25, 0.75) and (0.75, 0.75, 0.75). The Fi atoms located at (0.5, 0.5, 0.5) compensate the excess charge. The Hubbard term is applied only to the 4f states of Praseodymium and is taken to be 5 eV [27].

3. Results and Discussions

3.1. Structural properties

3.1.1. PrF_3

Praseodymium trifluoride PrF_3 crystallizes in the hexagonal tysonite

structure and adopts the space group $P\bar{3}c1$. In this structure, two parameters are optimized a, and the report c/a. Calculations show that the minimum energy corresponds to the values: $a = 6.877\,\text{Å}$ and $c = 7.178\,\text{Å}$. The parameter c is in agreement with that of the references [26] and [27]. The parameter "a" is also close to the reference [26] but differs by 41% from the results reported by Saini et al. [27] ($6.877\,\text{Å}$ versus $4.085\,\text{Å}$). The compressibility modules and their derivatives are calculated for the first time. The values obtained are $B = 153.756\,\text{GPa}$ and $B' = 4.766$ (Table 1).

Table 1. Calculated lattice constants (Å), R_{MT} and bulk modulus (GPa) in both PrF_3 and $Sr_{0.75}Pr_{0.25}F_{2.25}$

Materials	Lattice constants Å				Exp.	Bulk Modulus (GPa)		Exp.	R_{MT}
	Theoretical					Theoretical			
	Present		Others			Present	Others		
PrF_3	a= 6.877	c= 7.1783	a= 6.87[b]	c= 4.08[b]	a=6.987[a] c=7.172[a] [26][a]	153.756	109.262	/	Pr : 2.26 F : 2
$Sr_{0.25}Pr_{0.75}F_{2.25}$	a= 5.6667		/		a=5.81[c]	109.262	/	/	Pr : 2.3 Sr : 2.17 F : 2.04

[a]Ref. [26], [b]Ref. [27], [c]Ref. [28]

3.1.2. $Sr_{0.75}Pr_{0.25}F_{2.25}$

The compounds $Sr_{0.75}Pr_{0.25}F_{2.25}$ are obtained by mixing in stoichiometric proportion the fluoride SrF_2 with the trifluoride PrF_3. $Sr_{0.75}Pr_{0.25}F_{2.25}$ crystallizes in the cubic structure and adopts the space group $Pm\bar{3}m$. The parameter that corresponds to the minimum energy is equal to $5.66\,\text{Å}$ (Table 1) which is close to the experimental value found

by J. Meuldijk et al. [28]. The compressibility modules and their derivatives are calculated for the first time and are equal to: $B = 109.262$ GPa and $B' = 5.546$ (Table 1). To our knowledge, no theoretical calculations have been performed on these compounds.

3.2. Electronic properties

We calculate the band structure of the compounds PrF_3 and $Sr_{0.75}Pr_{0.25}F_{2.25}$ using both approximations: local density spin approximation LSDA and Coulomb-corrected local spin density approximation LSDA + U. The last one is used to note the Hubbard term U influence on the f-states.

3.2.1. PrF_3

3.2.1.1. Band structures

Figure 1 shows the band structures for both spin up and down. This figure exhibits a clear difference between the spin up and down band structures for each approximation.

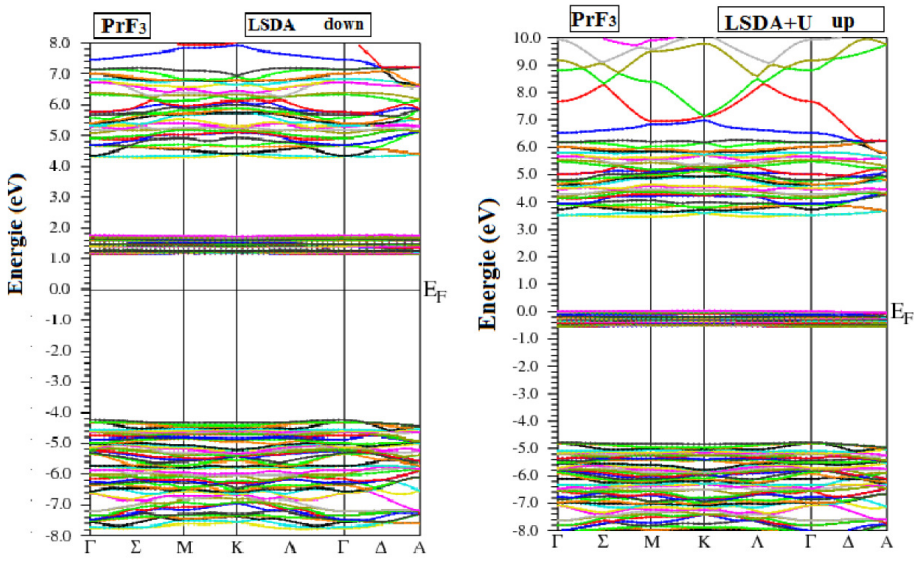

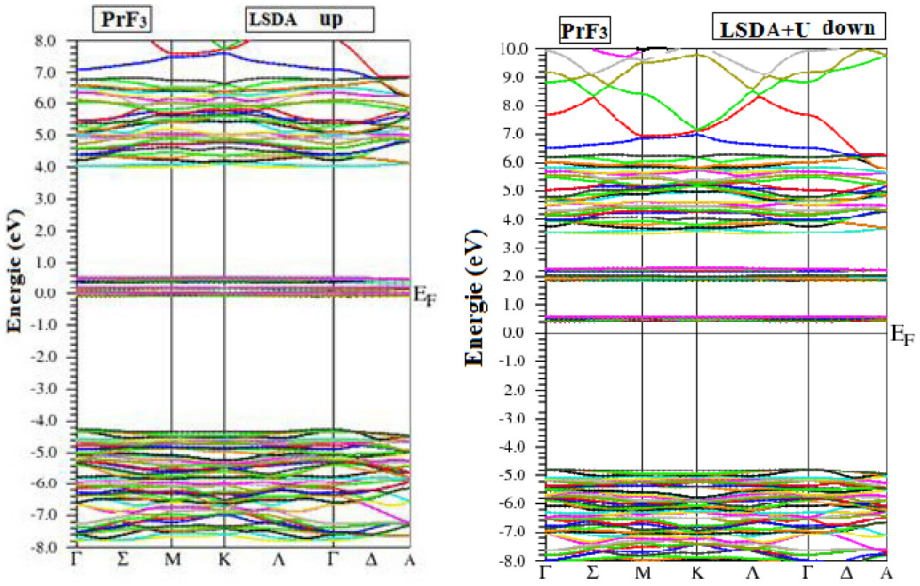

Figure 1. Band structure of the PrF_3 compound using LSDA and LSDA + U approximations.

For the spin up (LSDA), the f-states are on the Fermi level giving to an incorrect metallic character. For spin down, the unoccupied f-states are at 1.2 eV above the Fermi level and the occupied f-states are found around 4.8 eV. A direct energy gap of 5.39 eV (Table 2) is observed at Γ point. With the DFT + U approach, for the spin up, the f states are also on the Fermi level maintaining a metallic nature. While for the spin down, the f-states are pushed from the Fermi level leading to a direct gap of 5.21 eV (Table 2) at Γ point comparable to that obtained with LSDA. This indicates the influence of this approach for treating the strongly correlated 4f electrons. Although the LSDA removes the f-states from the Fermi level, it is unable to elevate the degeneration of these states.

The gap obtained with the DFT + U approach differs from that of reference [27] (5.21 versus 6.69 eV). This is due to the difference between the values of the crystalline parameter *c* used (7.18 versus 4.08 Å).

Indeed, it is well known that the gap is inversely proportional to the crystalline parameter [29].

3.2.1.2. Density of state (DOS)

The total density of state (DOS) (up and down) using both LSDA and LSDA + U approximations is shown in Figure 2. The conduction band is made by both Pr-f and Pr-d. The Pr-f present sharp peaks and are highly localized while the Pr-d form a broad band. The valence band is constituted by both Pr-p and F-p. One can notice that, for the spin up there is no appreciable difference between the two approximations. On the other hand, for the spin down, the density is zero at the Fermi level for both approximations giving rise to an insulating nature in PrF_3.

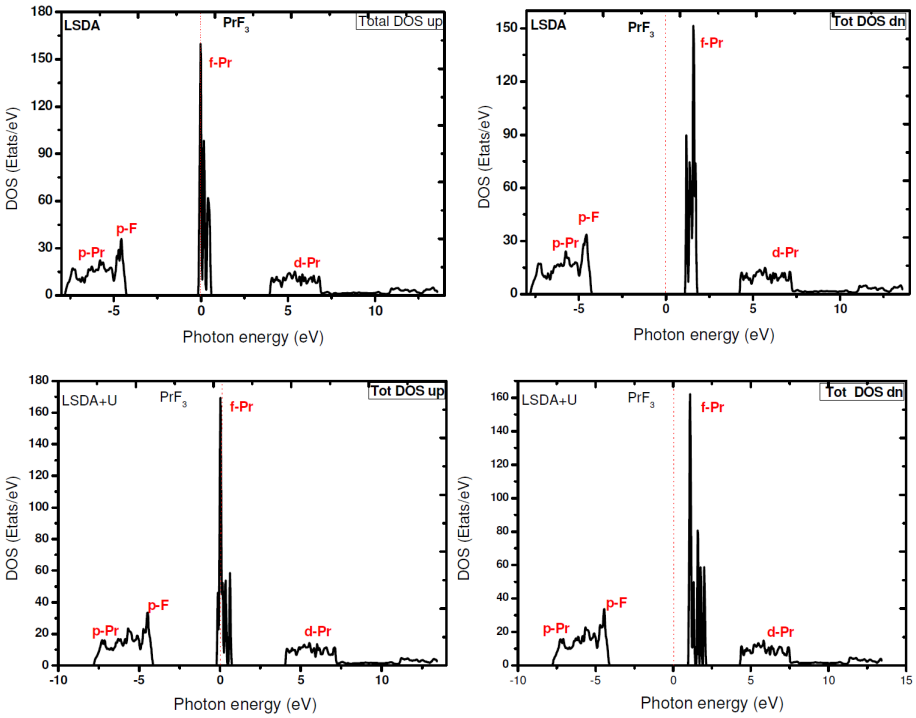

Figure 2. Total state density of the compound PrF_3 using approximations LSDA and LSDA + U.

3.2.2. $Sr_{0.75}Pr_{0.25}F_{2.25}$

3.2.2.1. Band structures

The band structures of the $Sr_{0.75}Pr_{0.25}F_{2.25}$ were calculated along the lines of high symmetry in the first irreducible Brillouin zone using both approximations LSDA and LSDA + U (Figure 3). With LSDA, for spin up, we notice that both valence and valence bands overlap leading to a metallic behavior. For spin down, a semiconductor character is observed with a direct energy-gap of 3.0 eV at the point Γ (Table 2). Using LSDA + U, for spin up, we can see that some energy levels have been shifted away from the Fermi level but there is a small overlap between the valence and the conduction bands giving rise to a metallic nature. On the other hand, LSDA + U, for spin down, shows that the energy-gap is also direct (Γ - Γ) of 5 eV (Table 2). It is well known that fluorides (host matrix) doped rare earth ions leads to materials with a gap smaller than that of the host matrix. Indeed the rare earth ions energy levels are located in the forbidden band of the host matrix: SrF_2 energy-gap is around 11.75 eV [30-32] and it is equal to 5 eV for $Sr_{0.75}Pr_{0.25}F_{2.25}$ (LSDA + U).

Table 2. Band energy gap in both PrF_3 and $Sr_{0.75}Pr_{0.25}F_{2.25}$

Materials	Band gap (eV)				Other
	Theoretical				
	Present				
	LSDA		LSDA+U		
	Spin-up	Spin-down	Spin-up	Spin-down	
PrF_3	Metal	5.39	Metal	5.21	6.69[a]
$Sr_{0.25}Pr_{0.75}F_{2.25}$	Metal	3.00	Metal	5.00	/

[a]Ref. [27]

We notice that the LSDA + U do not exhibit a significant influence on the 4f electrons in the spin up channel.

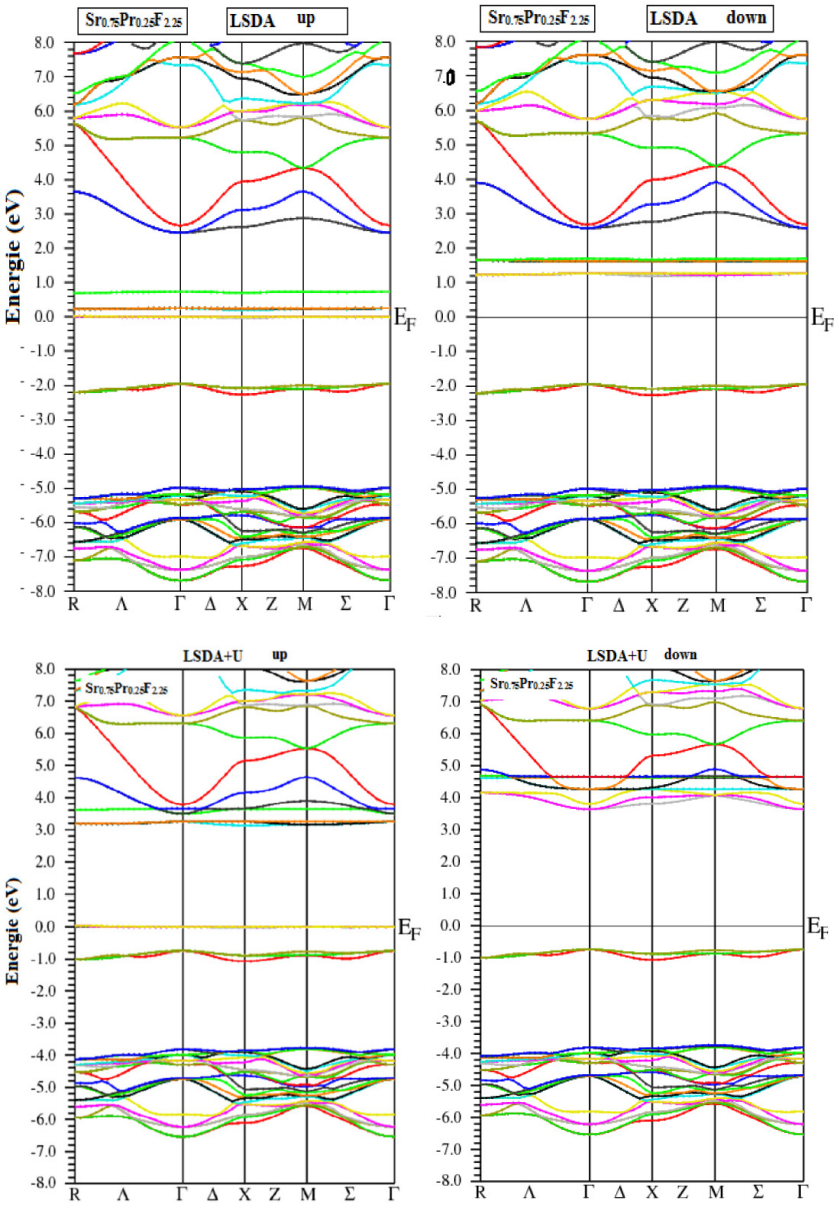

Figure 3. Band structure in $Sr_{0.75}\ Pr_{0.25}\ F_{2.25}$ using LSDA et LSDA + U approximations.

3.2.2.2. Density of state

Using LSDA approximation, for the spin-up, the Pr-f states are centered around the Fermi level and for the spin-down these states are grouped in the interval [1-1.7] eV (Figure 4). For both spin states, the top of the valence band is occupied by the Fi-p states and in the lower bands are found the Sr-d states. In the conduction band, we find the Pr-d and Sr-d states. Except for the f bands, the position of the other states does not depend on the nature of the spin. The curves obtained by LSDA + U for spin up have the same behavior as those obtained by LSDA. The position of all states (except f) remains unchanged for both spin states. On the other hand, the Pr-f states are between 1.26 and 1.64 eV. The splitting of the f levels is often found in rare earths when using LSDA + U [31]. Figure 4 shows that the f states intensity using LSDA are more important than that obtained with LSDA + U around the Fermi level. Indeed the shift of f states with LSDA + U naturally leads to a decrease in the density of states.

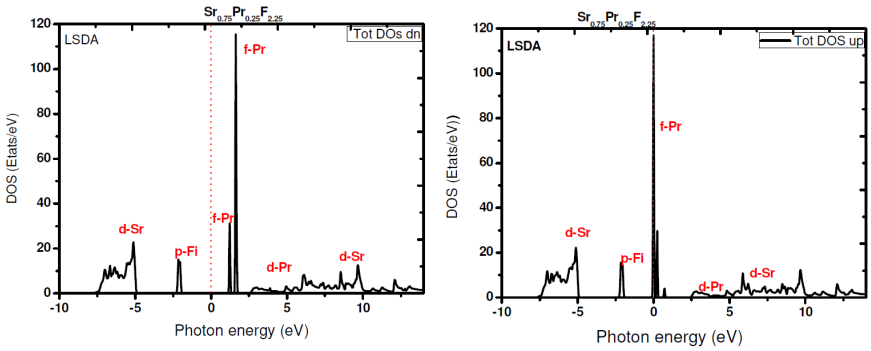

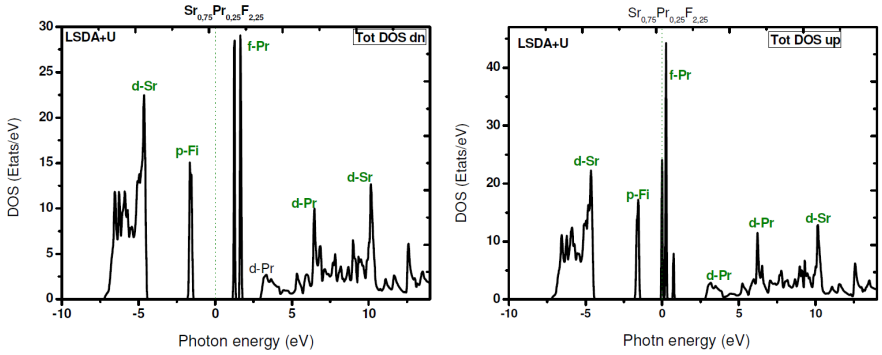

Figure 4. Total Density of state in $Sr_{0.75}\,Pr_{0.25}\,F_{2.25}$ using LSDA and LSDA + U approximations.

3.3. Optical properties

The optical properties of PrF_3 and $Sr_{0.75}\,Pr_{0.25}\,F_{2.25}$ are studied using both LSDA and LSDA + U approximations in the energy range from 0 to 40 eV. Optical properties derived from the dielectric function $\varepsilon(\omega)$, such as the refractive index $n(\omega)$, the absorption coefficient $\alpha(\omega)$, the extinction coefficient $k(\omega)$, the reflectivity $R(\omega)$ and the spectrum $L(\omega)$ which represents the electron energy loss function (Electron Energy Loss Spectroscopy, EELS) will also be investigated.

3.3.1. PrF_3

3.3.1.1. Real part of the dielectric function

Figure 5.1 shows the variation of the two components ε_{1xx} and ε_{1zz} as a function of the incident photon energy using both LSDA and LSDA + U approaches. The static values $\varepsilon_{1xx}(0)$ and $\varepsilon_{1zz}(0)$ are 197 (LSDA) and 51 (LSDA + U) and 185 (LSDA) and 83 (LSDA + U), respectively (Table 3). One can notice that the values obtained with LSDA are greater than those obtained with (LSDA + U). This can be explained by the fact that PrF_3 exhibits a metallic character (LSDA). The curves $\varepsilon_1(\omega)$ are almost similar for both approximations with some differences in

the range [0-6] eV. Both components of $\varepsilon_1(\omega)$ decrease from the static value $\varepsilon_1(0)$; ε_{1xx} is cancelled and becomes negative in the interval [0.13-0.99] eV with LSDA and [0.12-0.53] eV with LSDA + U, with depths of -−23.8 (a.u) with LSDA and −2.22 (a.u) with LSDA + U. While for ε_{1zz} it is cancelled and becomes negative in the interval [0.22-1.57] eV with LSDA and in [0.28-1.2] eV with LSDA + U with depths of −22.33 (a.u) with the LSDA and −4.16 (a.u) with LSDA + U. Then both components ε_{1xx} and ε_{1zz} increase to reach the following maximum values:

For ε_{1xx} : 5.06 eV (LSDA) and 4.2 eV (LSDA + U) and for ε_{1zz} : 5.14 eV (LSDA) and 4.43 eV (LSDA + U). We notice that the maxima obtained by the LSDA + U approximation are slightly shifted towards the low energies. In the spectral region [6-40] eV, the curves with both approximations LSDA is LSDA + U are almost similar. The first peak is at 8.97 eV (ε_{1xx}) and 9.20 eV (ε_{1zz}). After this peak, a decrease is observed and ε_{1xx} cancels and becomes negative in the interval [12.07-14.21] eV, and in [11.87-13.67] eV for ε_{1zz}. Then $\varepsilon_1(\omega)$ increases again and reaches a second maximum localized around 21.09 eV for ε_{1xx} and 21.17 eV for ε_{1zz}. Again $\varepsilon_1(\omega)$ cancels and takes negative values in both intervals [23.51-32.59] eV for ε_{1xx} and [23.08-33.14] eV for ε_{1zz}. It should be remembered that electromagnetic waves cannot propagate in these spectral regions [33].

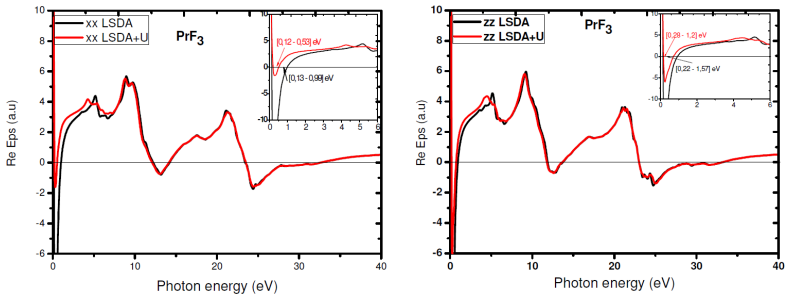

Figure 5.1. Real part of dielectric function of PrF_3.

3.3.1.2. Refractive index

The variation of the refractive index $n(\omega)$ as a function of the incident photon energy is shown in Figure 5.2. The static values of $n_{xx}(0)$ are: 16.60 (LSDA) and 8 (LSDA + U) and those of $n_{zz}(0)$ are: 15.75 (LSDA) and 10.75 (LSDA + U) (Table 3). It can be seen that the values obtained by (LSDA + U) are smaller than those obtained by LSDA in accordance with the results found for the dielectric constant at zero frequency (Table 3). In the spectral region [0-6] eV, differences related to the shift of peaks obtained with LSDA towards high energies with respect to LSDA + U for both components of the refractive index are observed. It is also noticeable that the curves have the same behavior for both approximations in the interval [6-40] eV. $n_{xx}(\omega)$ undergoes rapid decreases for the energies: 12.71 eV, 24.13 eV, and $n_{zz}(\omega)$ for the following energies: 11.93 eV, 23.35 eV and 24.67 eV. These values should correspond to the maximum absorption values (Figure 5.4).

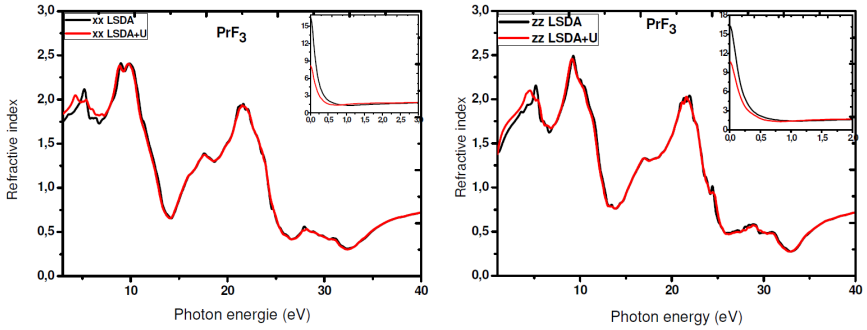

Figure 5.2. Refractive index of PrF_3.

3.3.1.3. Reflectivity

Figure 5.3 shows that the reflectivity curves are almost identical for both approximations. The peaks are grouped in two domains: the first extends from 2 to 20 eV and contains many peaks; the most intense is located at about 13.0 eV (30%). In the second domain, ranging from 20 to

40 eV, there are also a number of peaks; the most intense is situated around 25 eV (45%). Note that these values correspond to frequencies where $\varepsilon_1(\omega)$ is negative. A high reflectivity would prevent the waves from penetrating into the material and therefore will not be able to propagate [29]. The zero frequency reflectivity values obtained with LSDA + U (68%) are lower than those obtained with LSDA (85%). This may be due to the f states at Fermi energy indicating a metallic compound. Based on the spectra, a difference between the components R_{xx} and R_{zz} in the spectral intervals [0-7.5] and [24-33] eV is observed indicating the anisotropy and/or birefringence of the material in these areas.

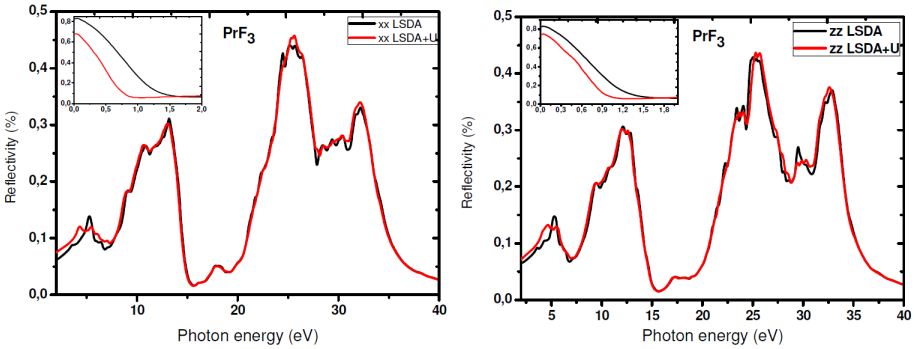

Figure 5.3. Reflectivity of PrF_3.

3.3.1.4. Absorption

The absorption spectra $\alpha(\omega)$, illustrated in Figure 5.4, show three bands. The first one is located in the spectral range [0-8.0] eV. In this region, the intensity of the first peak near 0.45 eV is even greater with LSDA than with LSDA + U (18×10^4 vs 8.6×10^4). Beyond 8 eV, the curves obtained with both approximations are almost identical. The second band is located around 12 eV and finally the third one, which contains the most intense peak, is found around 24 eV (the *x*-direction), but in the *z*-direction there is a double peak (23.35 and 24.67 eV).

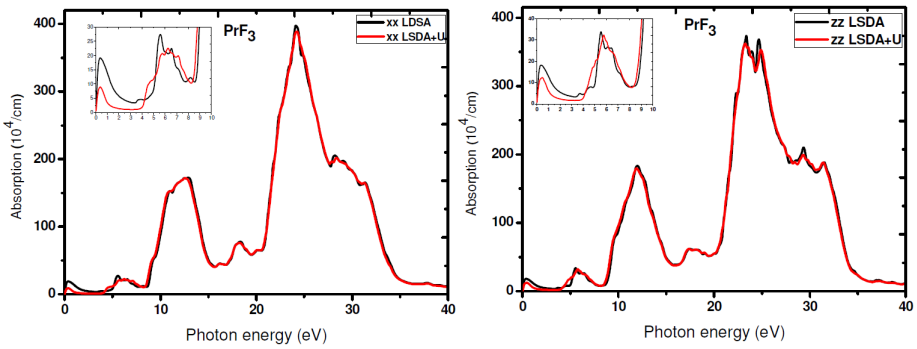

Figure 5.4. Absorption of PrF_3.

3.3.1.5. Electron energy loss function

We remember that the electron energy loss function $L(\omega)$ is defined as the energy lost during the inelastic interaction of fast electrons with the medium and is given by the relation $Im\dfrac{1}{\varepsilon(\omega)} = \dfrac{\varepsilon_2(\omega)}{\varepsilon_1^2(\omega)+\varepsilon_2^2(\omega)}$ where $\varepsilon_1(\omega)$ and $\varepsilon_2(\omega)$ are real and imaginary part of the dielectric constant $\varepsilon(\omega)$.

The electron energy loss as a function of the incident photon energy is presented in Figure 5.5. Three energy bands are reported for the two components $L_{xx}(\omega)$ and $L_{zz}(\omega)$: the first one ranges from 0 to 3 eV, for $L_{xx}(\omega)$ in which we notice that the intensities are almost equal with a slight shift of the peak towards the high energies of the LSDA compared to the LSDA + U. The second band is between 8 and 27 eV, there is no difference between the two approximations and the most intense peak is located at about 14.35 eV. The third band containing the main peak (33.0 eV) extends from 27 to 40 eV. It can be seen that the peak intensity calculated with LSDA + U is slightly higher than that calculated with LSDA. For $L_{zz}(\omega)$, there are also 3 bands. In the first [0-3] eV, the intensity obtained with LSDA + U is slightly higher than that obtained with LSDA with always a shift of the peak towards high energies

compared to LSDA + U. Between 3 and 40 eV the curves are almost identical for both approximations. The maximum peaks in the second and third spectral region are found around 14 eV and 33 eV, respectively. The values of the main peaks (33 eV) represent plasma excitation and correspond to zero values of the real part of the dielectric constant $\varepsilon_1(\omega)$ and a low value of the imaginary part $\varepsilon_2(\omega)$ [34].

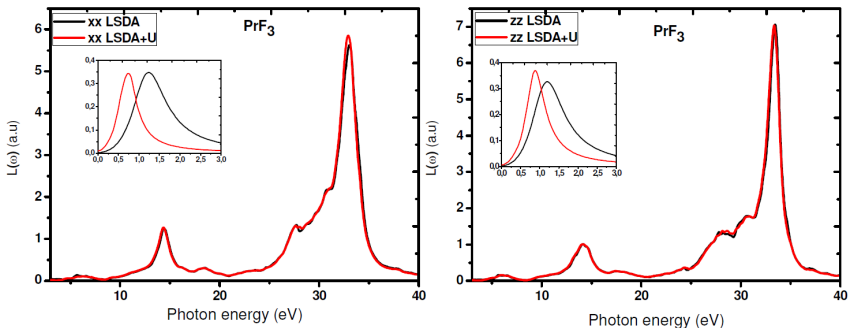

Figure 5.5. Energy Loss function of PrF_3.

3.3.2. $Sr_{0.75}Pr_{0.25}F_{2.25}$

3.3.2.1. Real part of the dielectric function

The variation of the real part of the dielectric constant $\varepsilon_1(\omega)$ as a function of the energy of the incident photon using the two approaches LSDA and LSDA + U is illustrated in Figure 6.1. The static values $\varepsilon_1(0)$ are equal to 8.52 (LSDA + U) and 21.96 (LSDA) (Table 3). It is noted that the value obtained with LSDA + U is smaller than that obtained with LSDA (metallic nature). The shape of the curves $\varepsilon_1(\omega)$ is almost the same for both approximations, with some differences in the range [0-6] eV where there is a slight shift towards the high energies of LSDA + U compared to LSDA. From the static value, $\varepsilon_1(\omega)$ decreases and reaches a first minimum at 0.16 eV with the LSDA + U and 0.18 eV with LSDA, then increases to the following maximum values: 2.01 eV (LSDA), 2.63 eV (LSDA + U), 5.07 eV (LSDA) and 5.53 eV (LSDA + U). In the spectral

region [6-40] eV, the curves are almost identical. It is observed that a first minimum value is obtained for an energy equal to 15.16 eV; $\varepsilon_1(\omega)$ is negative in both spectral intervals [24-24.82] eV and [25-32] eV. It is well known that when $\varepsilon_1(\omega)$ is negative, the electromagnetic waves cannot propagate, consequently, the reflection coefficient is expected to reach a maximum value leading to a strong reflection in this spectral region [33].

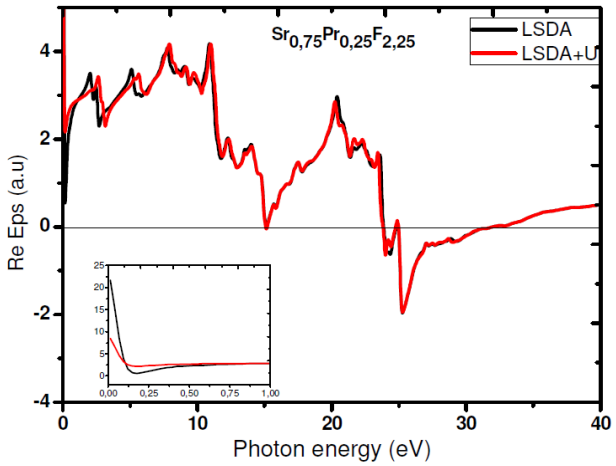

Figure 6.1. Real part of dielectric function of $Sr_{0.75}$ $Pr_{0.25}$ $F_{2.25}$.

3.3.2.2. Refractive index

The variation of the refractive index $n(\omega)$ is presented in Figure 6.2. This figure clearly shows that the static values obtained by LSDA + U (3.84) are smaller than those obtained by LSDA (6.79) (Table 3). We also notice that both curves have the same behavior for both approximations in the interval [6-40] eV. On the other hand, in the energy band [0-6] eV there are differences related to the shift of peaks obtained with LSDA + U to higher energies with respect to LSDA. We can see that $n(\omega)$ undergoes rapid decreases for energies: 11.46, 14.98 and 25.22 eV which correspond to maximum absorption. The static values of the real part of the dielectric function $\varepsilon_1(0)$ and of the refractive index $n(0)$ refraction of the three compounds are listed in Table 3.

Table 3. Static values of $\varepsilon_1(0)$ and $n(0)$ in PrF_3 and $Sr_{0.75}\ Pr_{0.25}\ F_{2.25}$

Materials	$\varepsilon_1(0)$				n(0)			
	LSDA		LSDA+U		LSDA		LSDA+U	
	xx	zz	xx	zz	xx	zz	xx	zz
PrF_3	197	51	185	83	16.5	15.75	8	10.75
$Sr_{0.75}Pr_{0.25}F_{2.25}$	21.96		8.52		6.79		3.84	

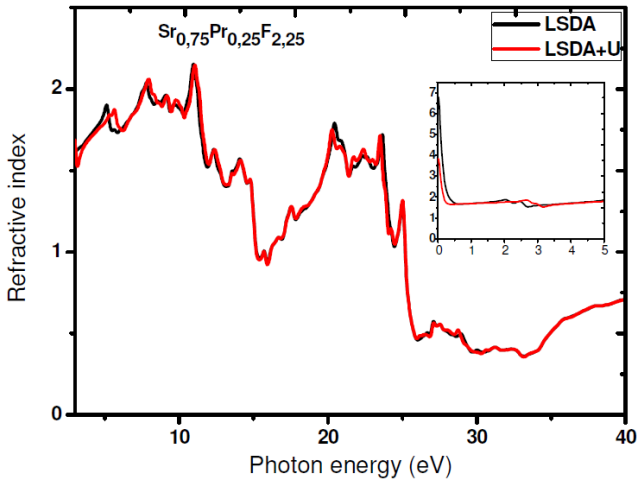

Figure 6.2. Refractive index of $Sr_{0.75}\ Pr_{0.25}\ F_{2.25}$.

3.3.2.3. Reflectivity

From the spectrum in Figure 6.3 it is clear that the values of reflectivity at 0 eV obtained with LSDA + U are lower than those obtained with LSDA. For high energies the curves are almost similar. The maximum peak is located at 25.78 eV (49%). We notice that this value is found in the spectral range [25-32] eV where $\varepsilon_1(\omega)$ is negative.

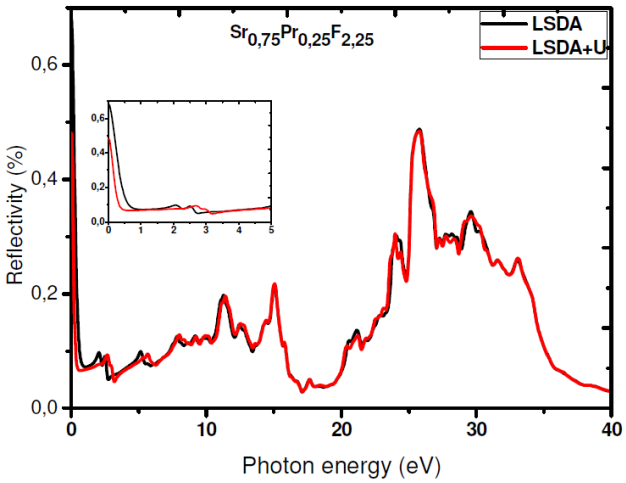

Figure 6.3. Reflectivity of $Sr_{0.75}$ $Pr_{0.25}$ $F_{2.25}$.

3.3.2.4. Absorption

The absorption spectrum (Figure 6.4) shows three bands: the first, in the spectral range [0-5] eV, presents three peaks, the most intense is positioned at 2.60 eV (LSDA) and 3 eV (LSDA + U), the second is found around 0.23 eV (LSDA), 0.15 eV (LSDA + U) and the third is located at about 2.16 eV (LSDA), 2.80 eV (LSDA + U). Our calculated results are in agreement with the experimentally reported data of reference [35]. In this region we can see that there is a shift of the curves obtained with LSDA + U with respect to LSDA to high energies. The second energy band from [5-19] eV contains two main peaks: the first at 11.46 eV and the second (the most intense) at 14.98 eV. In the third band [20-40] eV, there are two peaks with the strongest peak in the whole spectrum around 25.22 eV. We notice that in the spectral region [5-40] eV, both spectra obtained with both approximations are almost similar. This clearly means that the f-states do not exhibit a great influence on the spectra in the high energy regions.

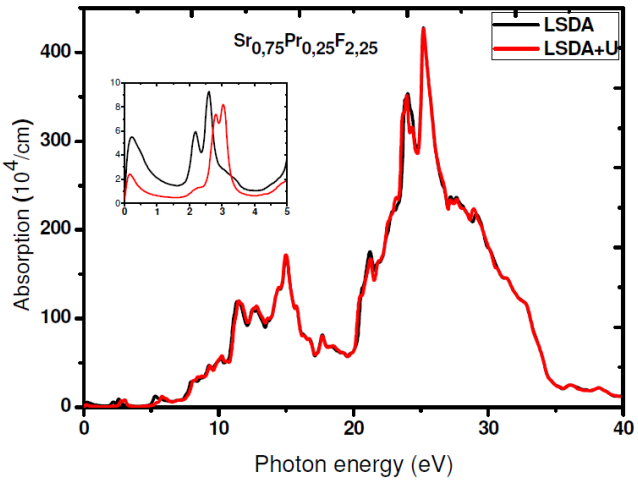

Figure 6.4. Absorption of $Sr_{0.75}\ Pr_{0.25}\ F_{2.25}$.

3.3.2.5. The electron energy loss function $L(\omega)$

The energy loss spectrum is shown in Figure 6.5 which reveals that in the interval [0-6] eV both spectra show differences related to the shift of peaks obtained with LSDA + U with respect to LSDA. In the spectral region [6-40] eV, the curves with both approximations LSDA and LSDA + U are almost identical. The most intense peak is around 33.23 eV. This result is in agreement with the plasma oscillation frequencies $\varepsilon_p(\omega)$. Indeed, this peak occurs around energies for which the imaginary part of the function reaches its minimum and the real part cancels [34].

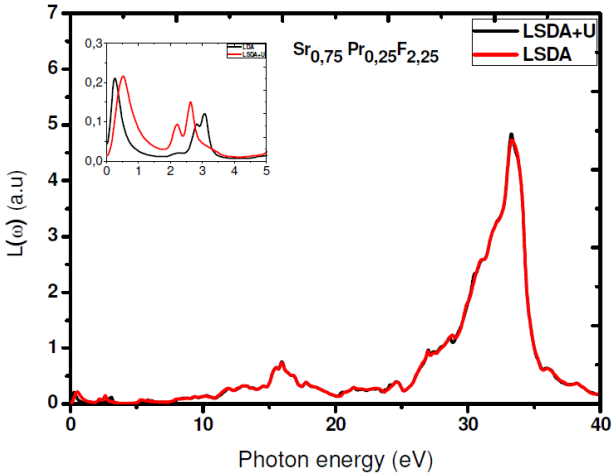

Figure 6.5. Energy Loss Function of $Sr_{0.75}$ $Pr_{0.25}$ $F_{2.25}$.

4. Comparison

From the Figure 7, it is clear that the optical curves in both SrF_2 (mBJ) [30] and $Sr_{0.75}$ $Pr_{0.25}$ $F_{2.25}$ (LSDA + U) have a common properties in the interval [0-11]. The figure reveals that $Sr_{0.75}$ $Pr_{0.25}$ $F_{2.25}$ has additional peaks in the SrF_2 band gap. The presence of these peaks shows the decrease of the doped fluoride $Sr_{0.75}$ $Pr_{0.25}$ $F_{2.25}$ energy-gaps. We remind that SrF_2 is a wide energy-gap [30-32] insulator whereas $Sr_{0.75}$ $Pr_{0.25}$ $F_{2.25}$ is also an insulator with a smaller gap. In the spectral range [11-40] eV, the curves are almost identical with shifts in energy. Wide-gap materials and especially fluorides-type MF_2 are widely used in spectroscopy as host matrices for rare earth ions [36] and investigated with various applications as laser spectroscopy [37-40], temperature sensors [41, 42], quantum information processing [43, 44], etc.

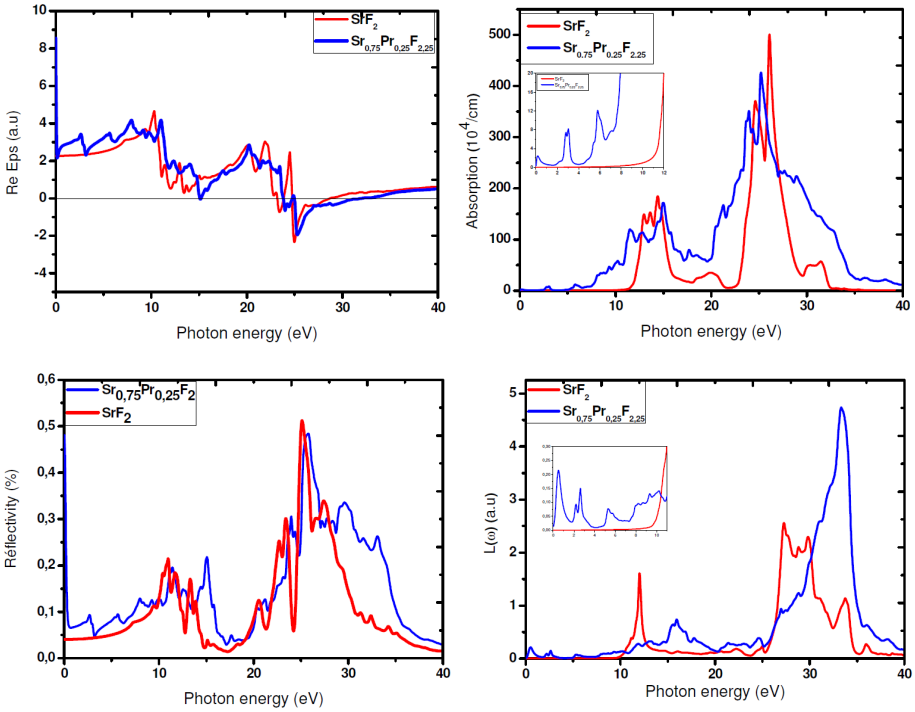

Figure 7. Comparison.

5. Conclusion

The lattice parameters and the compressibility modules at equilibrium have been calculated. The electronic properties study, using LSDA and LSDA + U, showed that PrF_3 is a metallic compound for the spin-up from both approximations and an insulator material for the spin-down. $Sr_{0.75}\ Pr_{0.25}\ F_{2.25}$ shows also a metallic material for the spin-up from both approximations while for the spin-down this compound exhibits an insulating energy-gap. The value gap for spin-down for both compounds and for both approximations are very close but the LSDA cannot elevate the f-levels degeneration unlike LSDA + U. $Sr_{0.75}\ Pr_{0.25}\ F_{2.25}$ gap is smaller than the gap of the no-doped fluoride SrF_2. This is due to the fact that the praseodymium energy levels are

within the band gap of the host matrix SrF_2. Optical properties such as the dielectric $\varepsilon(\omega)$ as well as the properties derived from it were also calculated. These calculations have shown that in the spectral range [11-40] eV the curves are almost identical but with energy shifts. On the other hand in the spectral range [0-11] eV the curves obtained for $Sr_{0.75}\,Pr_{0.25}\,F_{2.25}$ show additional peaks compared to those of SrF_2 indicating the inter-band transitions of praseodymium in this spectral range.

References

[1] A. Svane and O. Gunnarsson, Transition-metal oxides in the self-interaction-corrected density-functional formalism, Phys. Rev. Lett. 65 (1990), 1148-1151.

[2] M. Ernzerhofa and G. E. Scuseria, Assessment of the Perdew-Burke-Ernzerhof exchange-correlation functional, J. Chem. Phys. 110 (1999), 5029-5036.

[3] V. I. Anisimov, J. Zaanen and O. K. Andersen, Band theory and Mott insulators: Hubbard U instead of Stoner I, Phys. Rev. B 44 (1991), 943-954.

[4] V. I. Anisimov, I. V. Solovyev, M. A. Korotin, M. T. Czyzyk and G. A. Sawatzky, Density-functional theory and NiO photoemission spectra, Phys. Rev. B 48 (1993), 16929-16934.

[5] A. I. Lichtenstein, J. Zaanen and V. I. Anisimov, Density-functional theory and strong interactions: Orbital ordering in Mott-Hubbard insulators, Phys. Rev. B 52 (1995), R5467-R5470.

[6] A. Fujimori and F. Minami, Valence-band photoemission and optical absorption in nickel compounds, Phys. Rev. B 30 (1984), 957-971.

[7] J. Van Elp, R. H. Potze, H. Eskes, R. Berger and G. A. Sawatzky, Electronic structure of MnO, Phys. Rev. B 44 (1991), 1530-1537.

[8] P. W. Anderson, Localized magnetic states in metals, Phys. Rev. 124 (1961), 41-53.

[9] L. E. Nagel and M. O'Keeffe, Fast Ion Transport in Solids, W. Van Gool, ed., North Holland, Amsterdam, 1973.

[10] Z. I. Oftedal, About the crystal structure of tysonite and some artificially represented lanthanide fluorides, Phys. Chem. B5 (1929), 272-291.

[11] K. Schlyter, On the crystal structure of fluorides of the tysonite or LaF_3 type, Ack. Kern. 5 (1952), 73-82.

[12] K. Lee, Fluorine-19 Nuclear magnetic resonance in CeF_3, Solid State Commun. 7 (1969), 367-371.

[13] R. P. Bauman and S. P. S. Porto, Lattice vibrations and structure of rare-earth fluorides, Phys. Rev. 161 (1967), 842-847.

[14] M. Mansmann, The Crystal Structure of lanthanum trifluoride, Z. Kristallografiya 122 (1965), 375-398.

[15] A. Zalkin, D. H. Templeton and T. E. Hopkins, The atomic parameters in the lanthanum trifluoride structure, Inorg. Chem. 5 (1966), 1466-1468.

[16] I. Brach and H. Schulz, Determination of the diffusion path in the ionic conductor LaF3, Solid State Ionics 15 (1985), 135-138.

[17] A. K. Cheeham, B. E. F. Fender, H. Fuess and A. F. Wright, Acta Crystallogr. B 32 (1976), 94-97.

[18] H. E. Rast, H. H. Caspers, S. A. Miller and R. A. Buchanan, Infrared Dispersion and Lattice Vibrations of LaF_3, Phys. Rev. 171 (1968), 1051-1057.

[19] H. Sun, Qiwei Zhang, X. Wang and Chaoke Bulin, Strong red emission in Pr^{3+} - doped $(K_{0.5}Na_{0.5})NbO_3$ - $CaTiO_3$ diphase ceramics, J. Am. Ceram. Soc. (2014), 1-6.

[20] I. A. Boiaryntseva, A. V. Gektin, G. B. Stryganyuk, V. N. Bamer and A. N. Belsky, Emission centers in $Ca_{1-x}\,Pr_x\,F_{2+x}$ (x = 0.35) solid solutions, J. Appl. Spectr. 79 (2012), 589-594.

[21] Y. Boyarintseva, N. Shiran, A. Gektin, V. Nesterkina, K. Chimamura and E. Villora, Radiation stability of $M_{1-x}\,Pr_x\,F_{2+x}$ (M = Ca, Sr, Ba) crystals, Radiat. Meas. 45 (2010), 340-342.

[22] P. Tardy, Y. Deshayes et al., Study of $Ca_{1-x}\,Pr_x\,F_{2+x}$ solid solution thin films grown on silicon substrates, Thin Solid Films 347 (1999), 127-132.

[23] O. Greis and J. M. Haschke, Handbook on the Physics and Chemistry of Rare earths, North-Holland, Amsterdam 20, 1995.

[24] P. Blaha, K. Schwarz and J. Luitz, WIEN97, Vienna University of Technology Improved and updated Unix version of the original copyrighted WIEN code, which was published by P. Blaha, K. Schwarz, P. I. Sorantin and S. B. Trickey (1990), Comput. Phys. Commun. 59 (1997), 399-415.

[25] P. Hohenberg and W. Kohn, Inhomogeneous electron gas, Phys. Rev B. 136 (1964), 864-871.

[26] B. A. Maksimov, M. I. Sirota, R. Galiulin and B. Sobolev, The crystal structure of

PrF_3, and the twinning and symmetry of tysonite-like structures, Sov. Phys. Crystallogr. 30 (1985), 284-289.

[27] S. M. Saini, Thesis: Optical and magneto-optical properties of rare earth metals and compounds, Indian Institute of Technology, Roorky, 2007.

[28] J. Meuldijk, R. van der Meulen and H. W. den Hartog, Dielectric-relaxation experiments on cubic solid solutions of SrF_2 and CeF_3 or PrF_3, Phys. Rev. B. 29 (1984), 2153-2159.

[29] Y. Kulvitit, S. Rolland, R. Granger and C. M. Pelletier, Dielectric-relaxation experiments on cubic solid solutions of SrF_2 and CeF_3 or PrF_3, Rev. Phys. Appl.15 (1980), 1501-1504.

[30] R. Khemici, Z. Chouahda, L. Tairi, F. Semari, B. Amimour, S. Benlamari, H. Meradji and S. Ghemid, First principles calculations of the structural, electronic and optical properties of the mixed fluorides $Sr_xCd_{1-x}F_2$, Chin. J. Phys. 56 (2018), 1033-1044.

[31] R. Khenata, B. Daoudi, M. Sahnoun, H. Baltache, M. Rerat, A. H. Reshak, B. Bouhafs, H. Abid and M. Driz, Structural, electronic and optical properties of fluoritetype compounds, Eur. Phys. J. B 47 (2005), 63-70.

[32] N. Shiran, A. Gektin, V. Nesterkina, Y. Boyarintseva, V. N. Baumer, G. Stryganyuk, A. Voloshinovskii, K. Shimamura and E. Villora, Peculiarities of cascade photon emission and energy storage in $M_{1-x}\,Pr_x\,F_{2+x}$ $(M = Ca, Sr, Ba, x = 0.35)$ crystals, J. Lumin. 130 (2010), 2277-2280.

[33] C. Kittel, Physique de l'état solide, 5ème edition, Paris, 1983.

[34] F. Pradal, C. Gout and D. Fabre, Les pertes caractéristiques d'énergie des electrons dans les solides, J. Phys. 26 (1965), 372-384.

[35] G. Liu and B. Jacquier, Springer Science and Business Media, 2006.

[36] N. M. Idris, M. K. Gnanasammandhan, J. Zhang, P. C. Ho, R. Mahendran and Y. Zhang, In vivo photodynamic therapy using upconversion nanoparticles as remotecontrolled nanotransducers, Nat. Med. 18 (2012), 1580-1585.

[37] M. Salah Kamel, A. Khosa, A. Tawse-Smith and J. Leichter, The use of laser therapy for dental implant surface decontamination: a narrative review of in vitro studies, Lasers. Med. Sci. 29 (2014), 1977-1985.

[38] M. Bouffard, J. P. Jouart and M. F. Joubert, Red-to-blue up-conversion spectroscopy of Tm^{3+} SrF_2, CaF_2, BaF_2 and CdF_2. Opt. Mater. 14 (2000), 73-79.

[39] A. Ikesue, T. Kinoshita, K. Kamata and K. Yoshida, Fabrication and optical

properties of high-performance polycrystalline Nd: YAG ceramics for solid-state lasers, J. Am. Ceram. Soc. 78 (1995), 1033-1040.

[40] J. P. Jouart, C. Bissieux and G. Mary, Energy transfer up-conversion in $CdF_2 : Er^{3+}$ and $Sr_xCd_{1-x}F_2 : Er^{3+}$. J. Lumin. 29 (1984), 261-274.

[41] Z. Chouahda, T. Duvaut, J. P. Jouart and M. Diaf, Temperature rise monitoring through red-to-green up conversion in $Er^{3+} : Sr_{0.3}Cd_{0.7}F_2$ crystals, Opt. Mater. 30 (2008), 1044-1047.

[42] Z. Chouahda, J. P. Jouart, T. Duvaut and M. Diaf, The use of the green emission in Er^{3+} doped CaF_2 crystals for thermometry application, J. Phys. Condens. Matter. 21 (2009), 245504-1-245504-5.

[43] C. W. Thiel, T. Böttger, R. L. Cone, Rare-earth-doped materials for applications in quantum information storage and signal processing, J. Lumin. 131 (2011), 353-361.

[44] I. Gutzow, E. Zlatera, S. Angelov and S. Levy, Structure and properties of thermoluminiscent calcium fluoride glass ceramic materials, J. Mater. Sci. 24 (1989), 1281-1286.